Penetration of a negatively buoyant jet in a miscible liquid

Pierre Philippe, Christophe Raufaste, Pascal Kurowski, Philippe Petitjeans

Penetration of a negatively buoyant jet in a miscible liquid

P. Philippe,[a] C. Raufaste, P. Kurowski, and P. Petitjeans
Laboratoire de Physique et Mécanique des Milieux Hétérogènes, UMR CNRS 7636,
Ecole Supérieure de Physique et de Chimie Industrielles, 10 rue Vauquelin, 75231 Paris, France

(Received 14 June 2004; accepted 21 March 2005; published online 2 May 2005)

We report experimental results on the evolution of a laminar liquid jet injected with negatively buoyant condition in a miscible surrounding liquid. Since molecular diffusion is negligible, the only significant miscible effect is the absence of any surface tension. After an initial intrusion phase, the jet reaches a steady-state characterized by a constant penetration depth. A simple theoretical model is derived which successfully predicts the transient phase as well as the subsequent steady state in terms of stationary penetration depth and jet's profile. All the experimental points collapse on a master curve involving two dimensionless numbers: the densimetric Froude number Fr and *S*, a number comparing viscous friction to buoyancy. Finally, this curve obtained for laminar flows is compared to classical results on turbulent fountains. © *2005 American Institute of Physics*.
[DOI: 10.1063/1.1907735]

I. INTRODUCTION

A buoyant jet refers to the general situation of a fluid locally injected into another one.[1] The case of a downward flow in a lighter fluid, or of an upward flow in a denser fluid, is called a positively buoyant jet since inertia of the flow and buoyancy act together in the same direction. Inversely, a negatively buoyant jet corresponds to the reverse case where buoyancy is opposed to the injection flow. This arises in numerous industrial processes or natural flows such as refueling compensated fuel tanks on naval vessels,[2,3] waste disposal systems, ventilation of large buildings,[4] or motion of plumes and clouds in the atmosphere.[5]

In most of these situations, the Reynolds number is quite large and the flow becomes turbulent very close to the injection source. Such turbulent jets, or turbulent fountains, have been extensively studied. Their general behavior is independent of the Reynolds number Re and solely depends on the Richardson number Ri which compares inertia to buoyancy. Ri can be defined as $\mathrm{Ri}=g^{*}D/V^{2}$ where $g^{*}=g\Delta\rho/\rho$ is the reduced gravity between the jet and the ambient liquid, D the orifice diameter, and V the mean velocity of injection. Some authors also define this quantity as a densimetric Froude number constructed on D and equal to $\mathrm{Ri}^{-1/2}$. In the following, this terminology will be reserved for the use of a densimetric Froude number built not on the orifice size D but on the maximal penetration depth H. One of the main experimental results, first obtained by Turner, deals exactly with this penetration depth H of a turbulent jet and predicts a power law dependence with $\mathrm{Ri}:H/D\propto\mathrm{Ri}^{-1/2}$ for heavy salt jets in pure water.[4,5] This result is consistent with dimensional analysis assuming that momentum and buoyancy fluxes are the only relevant parameters in this problem.[4–6] Many other results in close situations, such as a denser liquid jet in pure water,[1,3,7–10] a liquid jet impinging on an interface,[2,3] or a turbulent heated air in ambient air,[11] suggest a similar power law relation. According to Friedman and Katz,[2,3] the exponent of the power law is $\approx -1/2$ when $\mathrm{Ri}<0.1$, but seems close to -1 for larger values of Ri.

To our knowledge, only a few studies have been dedicated to the case of laminar jets. In the particular situation of the impingement of an immiscible interface with a vertical jet, Friedman and Katz[2,3] obtained a power law $H/D\propto\mathrm{Ri}^{-1/3}$. For a numerical model of weak laminar fountains with Reynolds numbers ranging from 800 down to 5, Lin and Armfield[9,10] found for Ri the same power law as in the turbulent case but with an extra dependence on $\mathrm{Re}:H/D\propto\mathrm{Re}^{-1/2}\mathrm{Ri}^{-1/2}$. Nevertheless, both studies correspond to very small penetration depth ($H/D<2$) due to rather large values of $\Delta\rho/\rho$ in comparison to the ones used in our experiments. Moreover, in the situation investigated by Lin and Armfield, the difference of density comes from the difference of temperature between the injected fluid and the ambient fluid. This leads to thermal diffusion and, thus, H also depends on the Prandtl number Pr ($\mathrm{Pr}=\nu/\kappa_T$ with κ_T the thermal diffusivity). Contrariwise, thermal as well as molecular diffusions are negligible in our study. This means that the only significant miscible effect is the absence of surface tension at the interface between the outer and the inner liquids. Finally, we can also mention the work of Clanet[12] on pulsating fountains of water in air. But in this last case the surface tension leads to a very specific behavior and, here again, any comparison seems rather difficult.

In this paper, we present an experimental study of a liquid jet injected in a miscible surrounding liquid. The outer liquid is slightly denser than the inner one and in all the experiments the flow regime is laminar, except for a few experiments presented in the last section. The paper is organized as follows. After a description of the setup in Sec. II and of the experimental observations in Sec. III, a simple theoretical model is proposed in Sec. IV and provides a complete analytical solution. The dynamics of the head of the jet during the initial penetration phase is studied in Sec. V whereas Sec. VI is devoted to the subsequent steady-state

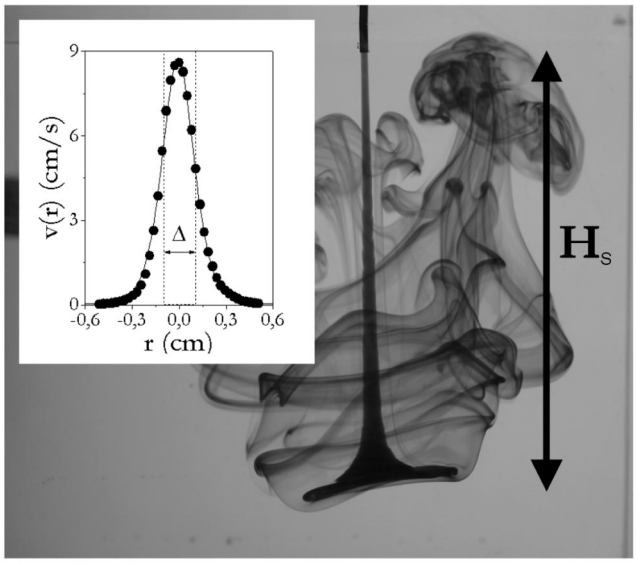

FIG. 1. Typical example of a steady jet: a liquid is injected downwards from a nozzle in a tank containing a slightly denser miscible liquid and reaches a stationary penetration depth H_s after a few seconds. Inset: example of a velocity profile obtained by PIV measurement at mid-height in the jet. The vertical dotted lines show approximately the boundary between the central jet of lighter liquid (diameter Δ) and its radial boundary layer. An approximate fit is also presented (see later for details).

regime with a particular focus on the shape and the maximal penetration depth of the jet. Finally, in Sec. VII, a general collapse is obtained in terms of dimensionless numbers and, a comparison with the case of turbulent fountains is presented.

II. EXPERIMENTAL SETUP

The experiments are performed as follows: a liquid of density ρ is injected downwards, at a constant volume flow rate Q, from a nozzle into a tank containing a miscible liquid of density $\rho+\Delta\rho$ with $\Delta\rho>0$. The injection is carried out by a syringe pump or by a siphon from a large storage tank. The flow rate Q was varied in a large range from ≈ 0.002 cm^3/s to about 20 cm^3/s. A picture of a typical experiment is presented in Fig. 1. The inner diameter D of the nozzle was also varied from 0.254 mm up to 4.83 mm; more precisely we have used seven different diameters: $D=0.254$ mm, 0.407 mm, 0.508 mm, 0.838 mm, 1.372 mm, 1.75 mm, and 4.83 mm. From the small values of the Reynolds number ($\mathrm{Re}=Q/\nu D<100$ see Sec. VII) and the quite large length L of the nozzle ($L=20$ mm, 30 mm, and 65 mm), we can deduce that the flow inside the nozzle is a fully developed Poiseuille flow[13] (strictly speaking, in all the cases, the entry length is smaller than the nozzle length L). In each experiment, we used two liquids with a small difference of density and of kinematic viscosity ν. But, as detailed later, the resultant buoyancy is proportional to $\Delta\rho$ whereas the viscous dissipation does not depend on the difference of viscosity but only on the absolute value of ν in each liquid. So, since the difference of viscosity between the two liquids is very small, we can consider that ν is almost uniform in the whole tank. Three different liquids have been used: pure water with kinematic viscosity $\nu_0=10^{-2}$ cm^2/s at 25 °C and two glycerin–water mixtures for which we measured a viscosity ratio ν/ν_0, respectively, equal to 2.0 and 3.7. In nearly all the experiments, the difference of density was obtained by adding a little amount of commercial ethanol (purity 95%) in the liquid of the jet except in two experiments where we used salt water in the tank and pure water in the jet. Since the latter situation yields identical results, the only relevant parameters characterizing the differences of properties between the two liquids are $\Delta\rho/\rho$ and ν (excluding any other parameter as the surface tension, for instance). All experiments are performed in the range $4\times10^{-4}\leqslant\Delta\rho/\rho\leqslant3\times10^{-2}$. The distance from the bottom of the nozzle to the free surface was kept nearly constant to about 1 cm even if it does not seem to have a significant influence on the jet. Finally, a few amount of dye (methylene blue) added to the injected liquid allows the visualization of the jet which is recorded either on a charge-coupled device camera at 25 images/sec or on a high-speed video camera (FastCam Super 10k from Photron) up to 250 frames/sec. Note that the presence of dye is taken into account in $\Delta\rho/\rho$. Several high-resolution pictures (4256×2848) as the one presented in Fig. 1 were also used to evaluate the radial enlargement of the jet with depth.

A few experiments have also been carried out to evaluate the velocity profile in the flow by particle image velocimetry (PIV) with the high-speed camera: both liquids are seeded with some tracers (plastic spheres of radius $d_p\approx60$ μm and density $\rho_p=1.03$ g cm^{-3}) and the tank is locally illuminated by a thin vertical laser sheet which is orientated perpendicularly to the camera and intercepts the jet axis. The light sheet thickness is about 0.1 mm. The verticality of the light sheet is easily obtained and the jet is precisely centered inside the sheet by a micrometric stage. However, as the light sheet thickness is not negligible compared to the quite small diameters of the jets, we can only access to mean velocity profiles averaged on the illuminated region. The images are recorded (at 250 frames/sec with a resolution of 540×480) and processed by the software DAVIS 6.2 with algorithms from Lavision. An example of a velocity profile obtained by this procedure is presented in the inset of Fig. 1.

III. OBSERVATIONS

The liquid jet penetrates in the tank and progressively slows down due to the opposing buoyancy force and to the viscous dissipation in the whole flow. During this transient phase of penetration, the jet remains thin and exhibits a large head. This head consists of a toric lobe structure which results from the viscous friction of the outer liquid initially motionless (see the insets within Fig. 2). Note that this shape is similar to thermal rising plumes as, for instance, the ones induced by local heating in a silicon oil[14] or in mantel convective flows.[15] After few seconds, the jet finally stabilizes and reaches a steady state with a constant penetration depth. When reaching the end of the jet, the liquid is radially expelled and then starts to slowly rise back to the top of the tank. In some experiments, the initial penetration phase was recorded with the fast-camera up to 250 frames per second. Then a space-time diagram of the vertical central line of the

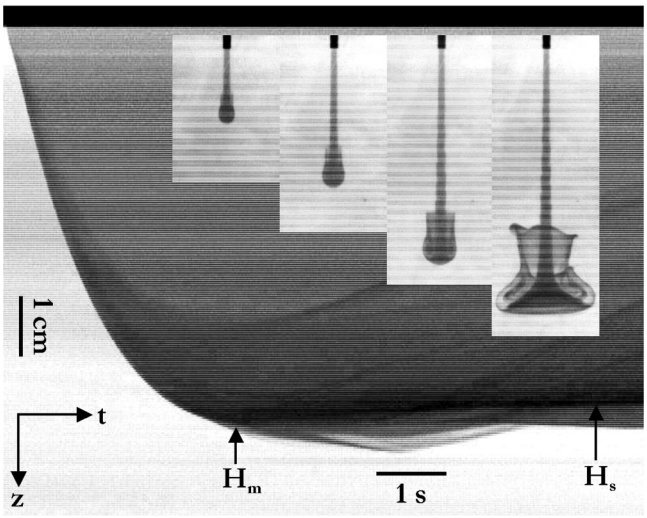

FIG. 2. Typical space-time diagram of the vertical central line of a jet. The jet progressively slows down until it reaches, within a few seconds, a stationary regime with a constant penetration depth. Here, $Q=0.127$ cm^3/s, $D=0.1372$ cm, $\Delta\rho/\rho=4.5\times10^{-3}$, and $\nu=\nu_0$. Insets: pictures of the jet during its transient penetration phase at $t=0.5$ s, 1 s, 2 s, and 4 s.

jet can be plotted. A typical example is shown in Fig. 2. We can accurately observe the transient regime of penetration, up to the maximal depth H_m, followed by the final steady state. We can notice that the stationary depth of penetration H_s is slightly smaller than H_m. This effect will be discussed later.

Some PIV measurements have been performed in the steady regime. A typical velocity profile is displayed on the inset of Fig. 1. The width of the profile is larger than the diameter of the jet and the profile exhibits a bell-shape in the central part of the jet with a large radial boundary layer outside. From the injection nozzle to the extremity of the jet, both the boundary layer and the central jet of the inner liquid progressively widen as can be seen in Fig. 1.

The control parameters are the injection flow rate Q, the internal diameter D of the nozzle, the relative difference of density between outer and inner liquid $\Delta\rho/\rho$, and the kinematic viscosity of both liquids ν. Qualitatively, when the three other parameters are fixed, an increase of each of D, $\Delta\rho/\rho$ or ν induces a decrease of the final penetration depth, whereas an increase of Q obviously produces the opposite effect.

As the density difference is produced by either ethanol or salt, the role of the molecular diffusion in the jet's flow studied here must be clarified. Three different length scales must be introduced to analyze this flow (see the sketch in Fig. 3). First, Δ is the width of the jet at a given depth z and corresponds to the width of the flow of the lighter liquid injected from the nozzle. Δ progressively widens with depth due to the mass conservation of the injected liquid and to the slowing down of the flow. This slowing down is caused by viscous damping and by the buoyancy force resulting from the small difference of density between the two liquids. So the widening of Δ is a purely hydrodynamic effect. The two other length scales are associated to momentum and molecular diffusion. δ_ν measures the length of the viscous boundary layer from the interface of the lighter liquid jet whereas δ_m is the length of the mixing layer at the interface between the injected liquid and the outer liquid caused by molecular diffusion of ethanol towards the outer liquid.

To know whether the molecular diffusion can be neglected or not, δ_m must be compared to Δ. This can be simply done in two steps. First, the comparison between δ_m and δ_ν gives directly,

$$\frac{\delta_m}{\delta_\nu}\sim\sqrt{\frac{\kappa_m}{\nu}}\sim S_c^{-1/2},$$

where κ_m is the molecular diffusivity and $S_c=\nu/\kappa_m$ is the Schmidt number.[13] The tabulated values for the molecular diffusivity of ethanol and salt are, respectively, at 25 °C: $\kappa_m\approx1.3\times10^{-5}$ cm^2/s and $\kappa_m\approx1.5\times10^{-5}$ cm^2/s. Consequently, the ratio δ_m/δ_ν is about 10^{-2}. Then we can now compare δ_ν with Δ by means of the PIV measurements. δ_ν is estimated on the velocity profile and Δ is measured using the contrast of luminosity induced by the dye. Clearly, δ_ν is the same order of magnitude than Δ (see the insets of Figs. 1 and 4). So, since $\delta_m/\delta_\nu\sim10^{-2}$ and $\delta_\nu\sim\Delta$, we can finally conclude that δ_m is much smaller than Δ and consequently the molecular diffusion of ethanol at the interface between the injected liquid and the outer liquid can be neglected. The same conclusion holds for salt diffusion since the molecular diffusivity of salt is nearly the same than the one of ethanol, and *a fortiori* for dye diffusion since the molecular diffusiv-

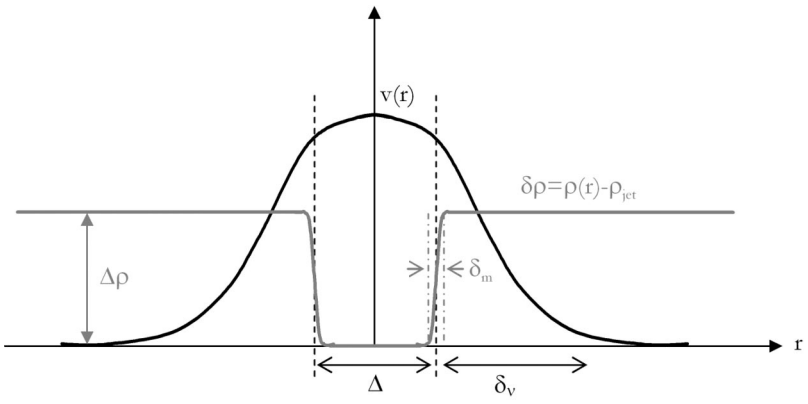

FIG. 3. Sketch of the flow at a given depth z: vertical velocity profile (black curve) and density profile (gray curve) with the three length scales involved in the flow Δ, δ_ν, and δ_m.

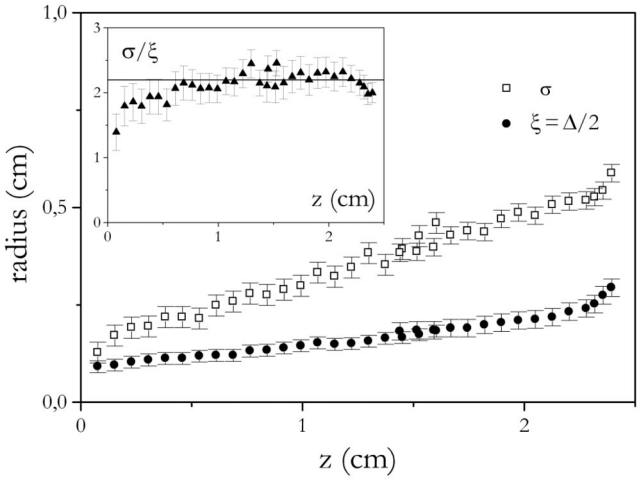

FIG. 4. Measurements along the flow of the radius of the jet $\xi=\Delta/2$ (●) and of the radius of the whole flow σ (□) obtained for $Q\approx 0.16$ cm^3/s, $D=0.175$ cm, $\Delta\rho/\rho=4.7\times10^{-3}$, and $\nu=\nu_0$. The criterion used to estimate σ is $v(\sigma,z)/v(0,z)\sim 0.1$. Inset: ratio σ/ξ as a function of the depth z (note that $\lambda\sim\xi/\sigma$ with λ defined in the text).

ity of methylene blue is one order of magnitude smaller than the one of ethanol ($\kappa_m\approx 1.7\times10^{-6}$ cm^2/s): this means in particular that the dye accurately tracks the lighter liquid and can be used to visualize the frontier between the jet and the viscous boundary layer.

To conclude with the role of molecular diffusion, it is important to underline that, generally speaking, a jet flow in a miscible fluid depends on the Schmidt number. But here, the flow corresponds to the limit of infinite Schmidt number where molecular diffusion is negligible. Another way to say it is that the flow has no significant miscible effect except at the interface between the outer and the inner liquids where there is no surface tension.

IV. THEORETICAL MODEL

A. Description of the model

Using the generalized theorem of Bernoulli, a simple theoretical model can be proposed to understand the penetration phase of the jet and the dependence of its stationary penetration depth and profile with the different control parameters: Q, D, $\Delta\rho/\rho$, and ν. Following the preceding discussion on diffusion, all diffusive processes are neglected in the model. Denoting the distance from a horizontal cross section of the jet to the exit of the nozzle as z, the difference of energy ΔE between z and $z=0$ is related to the viscous dissipation rate $W_\nu(z)$ by

$$\frac{d(\Delta E)}{dt}=W_\nu(z). \tag{1}$$

Seeing that the radial length scale D is negligible compared with the vertical length scale H, only the vertical velocity profile $v(r,z)$ will be considered in the following. We can also reasonably assume that the pressure inside the jet is equal to the hydrostatic pressure in the tank. Then the left-hand side of Eq. (1) reads

$$\frac{d(\Delta E)}{dt}=\int_0^\infty\frac{1}{2}\rho[v^3(r,0)-v^3(r,z)]2\pi r\,dr-Q\Delta\rho gz.$$

Since the viscosity is almost the same inside and outside the jet, the dissipation rate $W_\nu(z)$ is reduced to

$$W_\nu(z)=\int_0^z\int_0^\infty\eta\left(\frac{\partial v}{\partial r}\right)^2 2\pi r\,dr\,dz.$$

To go further, we use two practical assumptions. The first one concerns the velocity profile in the jet. This profile is not extensively known and only few PIV measurements have been realized. Moreover, a complete resolution of the Navier–Stokes equation seems quite complex. Nevertheless, as suggested by the bidimensional case,[13] we can reasonably assume the following separation of variables:

$$v(r,z)=V(z)\Psi[r/\sigma(z)]. \tag{H1}$$

Here $V(z)$ is the maximal velocity in the jet and Ψ corresponds to the radial dependency of the profile with $\Psi(0)=1$. $\sigma(z)$ is a scaling factor which accounts for the flow enlargement with depth. So $\sigma(z)$ is the characteristic width of the whole flow, including the jet and its viscous boundary layer.

A direct relationship between this characteristic viscous layer $\sigma(z)$ and the jet width $\Delta(z)$ would also be useful. The growth of the viscous boundary layer from the nozzle is proportional to $\sqrt{\nu t}$ where t is the transit time to reach a given depth z. So, $\sigma(z)-\Delta(z)/2\propto\sqrt{\nu t(z)}$ with t given by $t\sim\int_0^z dz'/v[r=\Delta(z')/2,z']$. Then, we can obtain the following implicit expression for the ratio $\Delta(z)/2\sigma(z)=\lambda(z)$:

$$[\lambda^{-1}(z)-1]^2\propto\frac{\nu}{\Delta^2(z)}\int_0^z\frac{dz'}{V(z')\Psi[\lambda(z')]}.$$

This implicit equation is strongly nonlinear and cannot be solved easily. Nevertheless, another way to extract a direct relationship between $\sigma(z)$ and $\Delta(z)$ is to use the PIV experiments. The procedure has already been discussed in the preceding section: Δ is measured using the contrast of luminosity induced by the dye and $\sigma(z)$ is estimated on the velocity profile. The results are presented in Fig. 4 [note that the criterion used to define $\sigma(z)$ at a given depth z is $v(\sigma,z)\sim v(0,z)/10$]. What we observe is that, far enough from the nozzle, λ is roughly constant which suggests that, in first approximation, there is a simple proportionality relation between $\sigma(z)$ and $\Delta(z)$. And so, this will be the second hypothesis of the model,

$$\sigma(z)=\frac{1}{\lambda}\frac{\Delta(z)}{2}, \tag{H2}$$

where λ is a constant strictly smaller than 1.

A reason for this result might come from the aspect ratio of the flow: the jet is indeed quite long compared to its diameter. So, from the exit of the nozzle, the flow is very likely to quickly reach an asymptotic state which simply gives rise to this proportionality relationship. This influence

of the aspect ratio may also explain why our results are quite different from the previous work on negatively buoyant fountains.[2,3,9,10]

From hypothesis (H1), the injection flow rate Q can be expressed as

$$Q = V(z)\sigma^2(z)\int_0^{\lambda(z)} \Psi(u) 2\pi u\, du.$$

Furthermore, using also hypothesis (H2) gives the following relation:

$$\gamma Q = V(z)\Delta^2(z), \tag{2}$$

where γ is a constant equal to

$$\gamma = 4\lambda^2 \Big/ \int_0^{\lambda} \Psi(u) 2\pi u\, du. \tag{3}$$

Then, with help of Eqs. (H1), (H2), and (2), Bernoulli theorem expressed in Eq. (1) becomes

$$Q\left\{\frac{1}{2}\rho\alpha[V^2(0) - V^2(z)] - \Delta\rho g z\right\} = \beta\eta\int_0^z V^2(z)dz, \tag{4}$$

with two coefficients, α and β, which depend only on the velocity profile. They can be directly expressed as

$$\alpha = \int_0^{\infty} \Psi^3(u) u\, du \Big/ \int_0^{\lambda} \Psi(u) u\, du, \tag{5}$$

$$\beta = 2\pi\int_0^{\infty} [\Psi'(u)]^2 u\, du. \tag{6}$$

Then, after derivation and integration of Eq. (4) over z, the expression of $V(z)$ is easily obtained. From here, the following nonlinear partial differential equation is derived for the penetration depth H by imposing the condition $V(z=H) = dH/dt$ at the head of the jet,

$$\frac{dH}{dt} = V(0)\sqrt{\left(1 + \frac{g^* Q}{\nu\beta V^2(0)}\right)e^{-(2\beta\nu/\alpha Q)H} - \frac{g^* Q}{\nu\beta V^2(0)}}, \tag{7}$$

where $g^* = (\Delta\rho/\rho)g$ is the reduced gravity and $\nu = \eta/\rho$ the kinematic viscosity in the whole liquid. $V(0)$ is the maximal velocity of the jet at the exit of the nozzle and, from hypothesis (H2), it is directly proportional to the flow rate Q since $\Delta(z=0) = D$:

$$V(0) = \gamma Q/D^2. \tag{8}$$

Using the change of variables $y = e^{-(2\beta\nu/\alpha Q)H}$, Eq. (7) can be solved analytically and gives the following expression for the transient penetration phase of the jet:

$$H(t) = H_m - a\frac{Q}{\nu}\ln\left[1 + \tan^2\left(\frac{t - t_m}{2a\gamma\dfrac{D^2}{\nu}\sqrt{b\dfrac{\nu Q}{g^* D^4}}}\right)\right]. \tag{9}$$

Equation (9) is valid for $t < t_m$ and, for $t > t_m$, $H = H_m$ where H_m is the maximal penetration depth of the jet and can be written as

$$H_m = a\frac{Q}{\nu}\ln\left(1 + b\frac{\nu Q}{g^* D^4}\right). \tag{10}$$

t_m corresponds to the transient time needed to achieve this maximal depth and reads

$$t_m = 2a\gamma\frac{D^2}{\nu}\sqrt{b\frac{\nu Q}{g^* D^4}}\arctan\left(\sqrt{b\frac{\nu Q}{g^* D^4}}\right). \tag{11}$$

Finally, the three following parameters $a = \alpha/2\beta$, $b = \beta\gamma^2$, and γ are introduced in the model and all of them can be expressed from the exact shape $\Psi(u)$ of the velocity profile.

B. Parameters of the model

So, the parameters a, b, and γ of the model only depend on the exact shape of the velocity profile. From Eq. (8) we can infer that $\gamma > 4/\pi$, which is the lower limit corresponding to a plug flow in the jet while a purely Poiseuille flow would give $\gamma = 8/\pi$. From the velocity profile shown in the inset of Fig. 1, we can note that the velocity of the flow at the frontier between the jet and its boundary layer is close to the maximal value $V(z)$. This means that the shape of the profile might be closer to a plug flow than to a Poiseuille flow and that γ must be only slightly larger than $4/\pi \approx 1.27$.

As an example, a further estimation of parameters α, β, and γ can be extracted from the velocity profile of Fig. 1. Using Eq. (6), we can directly evaluate β and obtain $\beta \approx 3.0$. Note that the profile can be satisfactory fitted by a Gaussian law or by a hyperbolic function inspired by the classical result of laminar bidimensional jet.[13] This latter fit is presented in Fig. 1 and corresponds to $\Psi(u) = 1/[\cosh(u)]^2$. Using these two fitting functions, the analytical calculus of Eq. (6) gives $\beta = \pi$ for the Gaussian law and $\beta \approx 0.87\pi \approx 2.73$ for the hyperbolic function. These values are in good agreement with the direct evaluation. As already presented in Fig. 4, it is also possible to correctly estimate the proportionality constant λ between the width of the flow and the diameter of the jet defined by Eq. (H2). Then, from Eqs. (5) and (3), we obtain values of α and γ in the range $\alpha \sim 1.1-1.4$ and $\gamma \sim 1.4-1.8$ which is, as mentioned before, a very reasonable value.

Finally, we can rather accurately fix the order of magnitude of the parameters:

$$a \sim 0.2, \quad b \sim 7, \quad \gamma \sim 1.6.$$

V. TRANSIENT PENETRATION

As already mentioned, the inverse buoyancy force and the viscous drag make the velocity of the liquid jet decrease while penetrating in the outer liquid. We have performed few sets of measurements in this transient regime for different experimental conditions. The temporal evolution $H(t)$ of the depth is obtained from space-time diagrams such as the one shown in Fig. 2. These have been compared to the theoretical expression of Eq. (9) for the transient dynamics of penetration $H(t)$. An example of comparison between the model and the experiments is presented in Fig. 5. Here we have used only one free parameter, namely, b: indeed, from the experi-

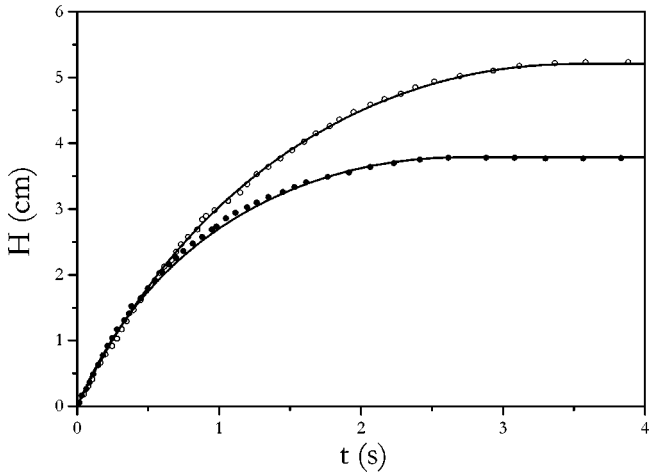

FIG. 5. Penetration of the head of the jet during the transient phase: (○) in the same experimental conditions as in Fig. 2 ($Q=0.127$ cm^3/s, $D=0.1372$ cm, $\Delta\rho/\rho=4.48\times10^{-3}$, and $\nu=\nu_0$); (●) for more viscous liquids ($Q=0.283$ cm^3/s, $D=0.175$ cm, $\Delta\rho/\rho=6.35\times10^{-3}$, and $\nu=3.7\nu_0$). The solid lines represent the prediction of the model with the following parameters: (○) $a=0.216$, $b=6.99$, and $\gamma=1.54$; (●) $a=0.189$, $b=7.21$, and $\gamma=1.72$.

mental measurements of both the maximal penetration H_m and the transient time t_m, Eqs. (10) and (11) give directly a and γ as functions of b. In this way, we have obtained values of a, b, and γ exactly in the range previously proposed. The agreement between the theory and the measurements is very good confirming the relevance of the assumptions made in the model, especially the two hypotheses (H1) and (H2).

VI. STEADY-STATE REGIME

A. Theoretical predictions

After the transient penetration of the jet, a steady state is reached where the penetration depth remains constant. As previously mentioned, this stationary depth H_s is slightly smaller than H_m, the maximal penetration depth of the jet at the end of its transient phase (see Fig. 2). This effect can be understood as follows: in the steady state, the liquid reaching the extremity of the jet is radially expelled and then starts rising back to the surface This slow backflow is governed by the negative buoyancy and slightly modifies the velocity profile of the boundary layer. So the viscous dissipation is expected to increase and thus the penetration depth to slightly decrease. We have also observed that the larger the difference of density, the larger the gap between H_m and H_s, which confirms this explanation. In the model, this effect could be taken into account by a small change of the parameters a and b in Eq. (10): b increases but a decreases so that H_s is slightly smaller than H_m.

Then the following nondimensional expression for H_s is obtained from Eq. (10):

$$\frac{H_s}{\lambda_0} = aS\ln(1+bS), \tag{12}$$

where we have introduced a nondimensional parameter

$$S = \frac{\nu Q}{g^* D^4} = \frac{Q}{Q_0}. \tag{13}$$

Note that this expression defines a characteristic flow rate, $Q_0=g^*D^4/\nu$, and a characteristic length directly built with Q_0: $\lambda_0=Q_0/\nu$.

The model gives a full prediction of the jet depth during the transient phase up to the final value H_s but it can also predict the shape of the jet in the steady-state regime. Indeed, from Eq. (2), $\Delta(z)$, the diameter of the jet (boundary layer not included) at depth z can be written as

$$\frac{\Delta(z)}{D} = \sqrt{\frac{\gamma Q}{V(z)D^2}}.$$

Then, using the expression of $V(z)$ obtained by integration of Eq. (4) (with the stationary condition $dH/dt=0$) and the expression of H_s given by Eq. (12), $\Delta(z)$ reads

$$\frac{\Delta(z)}{D} = (bS)^{1/4}[(1+bS)^{1-z/H_s}-1]^{-1/4}. \tag{14}$$

So, the model can give a complete description of the steady-state regime characterized by a constant penetration depth and a stationary profile which theoretical expressions are, respectively, given by Eqs. (10) and (14).

B. Stationary profile of the jet

In order to test these theoretical predictions, many experiments have been performed in the steady-state regime of the jet. The profiles $\Delta(z)$ are extracted from high-resolution pictures such as the one in Fig. 1. They can all be successfully fitted by expression (14) providing that D is replaced by a slightly smaller value D^*. This adjustment is simply due to the jet's contraction at the exit of the nozzle,[16] an effect which was neglected in the model. (Note that, strictly speaking, the origin $z=0$ used in the model does not exactly correspond to the exit of the nozzle but to the location of the maximal contraction of the jet just after it exits from the nozzle.) Some of these profiles $\Delta(z)$ are presented in Fig. 6.

As Eq. (14) depends only weakly on b, a direct fitting procedure fails to give a reliable value for b. So, we preferred to use a fixed value for b, namely, $b=7$. Then, the corresponding values obtained for D^* are in the range $0.9<D^*/D<0.94$ which appears realistic.[16]

C. Penetration depth

To test the theoretical expression of the penetration depth given by Eq. (8), we have made systematic measurements of H_s as a function of the flow rate Q in a large range of the different control parameters: D, $\Delta\rho/\rho$, and ν. As can be seen on Fig. 7(a), for a given couple of liquids, which corresponds to fixed values of $\Delta\rho/\rho$ and ν, it appears that the variation of H_s with Q is consistent with a power law. In all experiments, the exponent remains between 1.4 and 1.8 and the proportionality coefficient depends only on D. This dependence on D can be easily quantified by plotting the nondimensional depth H_s/D as a function of a characteristic velocity $U=Q/D^2$ which is directly proportional to the mean

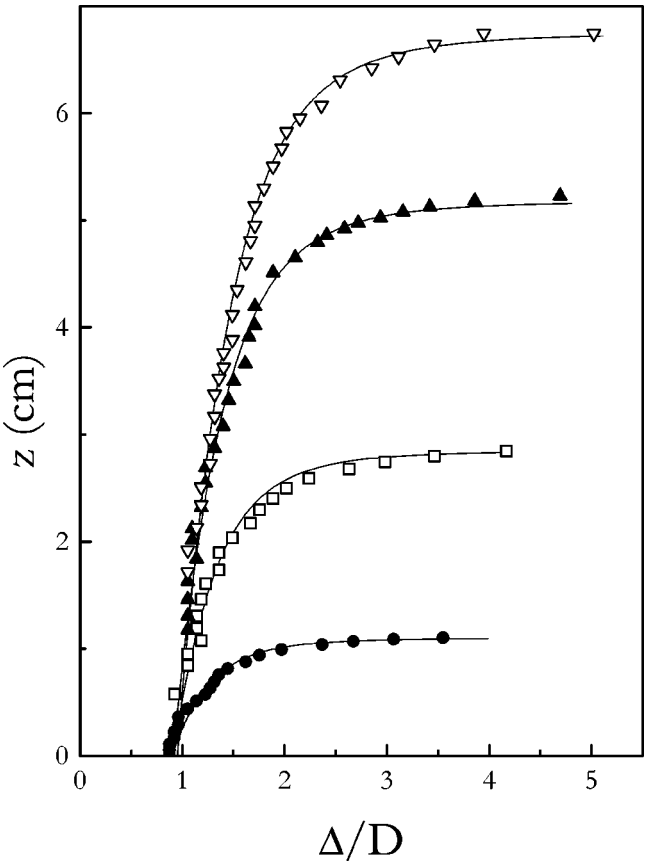

FIG. 6. Examples of jet profiles observed just after the steady state is reached under the same conditions ($D=0.137$ cm, $\Delta\rho/\rho=4.36\times10^{-3}$, and $\nu=\nu_0$) and for four different flow rates of injection: $Q=0.047$ cm^3/s (●), 0.086 cm^3/s (□), 0.132 cm^3/s (▲), and 0.151 cm^3/s (▽). The theoretical expression of the model is represented by the solid lines with the fixed parameter $b=7$ and $D^*/D=0.90$ (●), 0.91 (□), 0.91 (▲), and 0.94 (▽).

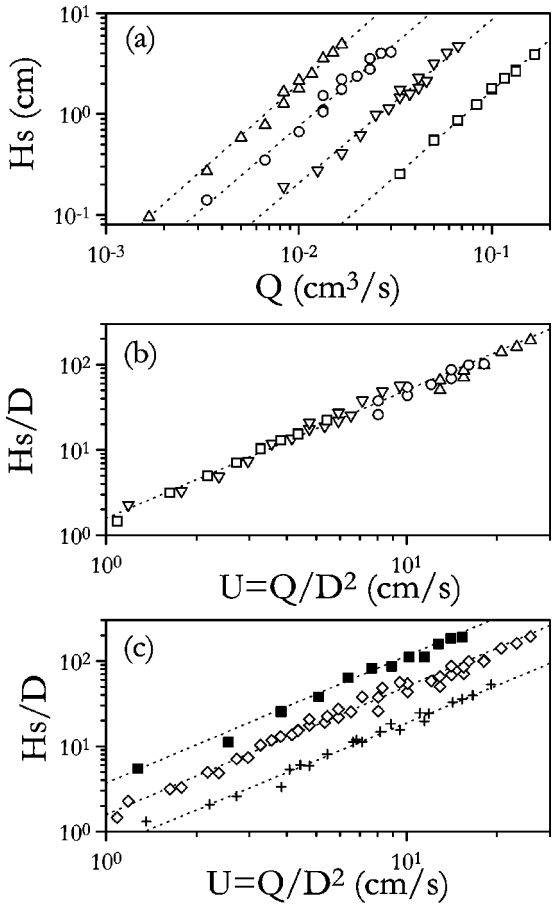

FIG. 7. (a) Dependence of the penetration depth H_s with the flow rate of injection Q with $\Delta\rho/\rho=4.48\times10^{-3}$ and $\nu=\nu_0$ and for four different nozzle diameters: $D=0.254$ mm (△), 0.407 mm (○), 0.838 mm (▽), and 1.75 mm (□). The dotted lines are power laws with, respectively, exponent 1.70 (△), 1.64 (○), 1.62 (▽), and 1.69 (□). (b) Collapse of the points presented in (a) by plotting the penetration ratio H_s/D as a function of the characteristic velocity $U=Q/D^2$. The dotted line is a power law with a new exponent 1.50. (c) Plots of H_s/D as a function of $U=Q/D^2$ for three different experimental conditions: $\Delta\rho/\rho=4.45\times10^{-4}$ and $\nu=\nu_0$ (■); $\Delta\rho/\rho=4.48\times10^{-3}$ and $\nu=\nu_0$ (◇) [same points as already presented in (a) and (b)], and $\Delta\rho/\rho=6.35\times10^{-3}$ and $\nu=3.7\nu_0$ (+). The dotted lines are power laws with exponent 1.49 (■), 1.50 (◇), and 1.46 (+).

injection velocity: the points collapse rather well on a master curve. This is shown in Fig. 7(b) and also in Fig. 7(c) where the data obtained in two other experimental conditions in terms of $\Delta\rho/\rho$ and ν have been added.

Then, all the collected data can be compared to the general nondimensional expression of Eq. (12). The result is presented in Fig. 8. It reveals that experimental points nicely collapse on a master curve and the following remarks can be made.

First, these results confirm that $H_s/\lambda_0=f(S=Q/Q_0)$ is quite a correct nondimensional form in a very large range of nearly four decades for H_s/λ_0 and six decades for $S=Q/Q_0$.

Second, the quantitative prediction of the model is very close to the experimental data except on both extremities of the graph: $S\leqslant10^{-2}$ and $S\geqslant10^{2}$. The theoretical curve presented in solid line in Fig. 8 was obtained with the typical values of the parameters: $a=0.2$ and $b=7$. The first significant discrepancy between the model and the measurements concerns the case $Q\ll Q_0$. This corresponds to experimental conditions where the jet becomes slightly turbulent and where the penetration depth starts to fluctuate. In Fig. 8, the maximal values of H_s is used. But, for these points, we can also estimate the mean penetration depth $\overline{H_s}$ by averaging H_s for a few ten of seconds. Then, if one replaces H_s by $\overline{H_s}$, a fairly better agreement is obtained between the theory and the experimental data as shown in the inset of Fig. 8. In the other extremity of the graph, i.e., $Q\gg Q_0$, we also observe a deviation between the experimental points and the model. These data correspond to the situation where $\nu=\nu_0$ and where we have used the thinner injection nozzle. So, as the collapse remains valid, this suggests that the model might still be used but with slightly different parameters. And maybe this is caused, at the exit of the nozzle, by a larger contraction of the jet when the diameter of the nozzle becomes smaller.[16]

Finally, a power law dependance between H and Q is suggested by the experimental results of Fig. 8. Despite the fact that Eq. (12) does not predict this behavior, an empirical power law can fit reasonably well the data on nearly all the experimental range. This empirical law is shown in dotted line in Fig. 7 and reads here

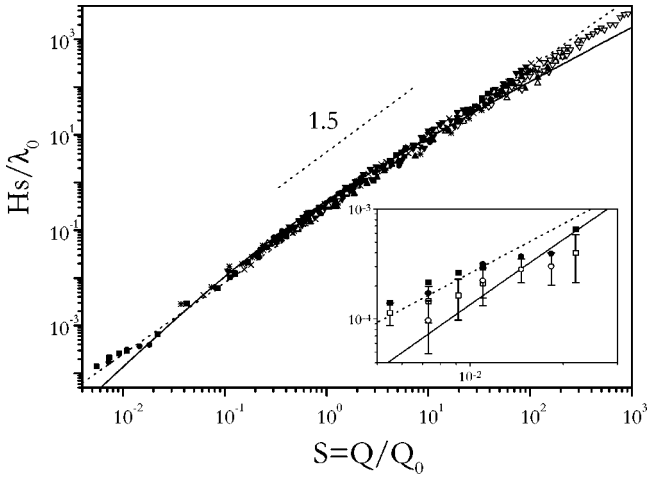

FIG. 8. Plot of the dimensionless depth H_s/λ_0 as a function of the flow rate ratio $S=Q/Q_0$ for many different experiments: (a) $\nu=\nu_0$ and $\Delta\rho/\rho=1.31\times10^{-2}$ (●), 8.13×10^{-3} (*), $=7.10\times10^{-3}$ (■), 4.48×10^{-3} (▼), 4.47×10^{-3} (×), 2.0×10^{-3} (+) (case of pure water injected in salt water), and 4.13×10^{-3}, 1.74×10^{-3}, 8.18×10^{-3} and 4.45×10^{-3} (▽); (b) $\nu=2.0\nu_0$ and $\Delta\rho/\rho=4.62\times10^{-3}$ (▲); (c) $\nu=3.7\nu_0$ and $\Delta\rho/\rho=6.35\times10^{-3}$ (△). The solid line corresponds to Eq. (12) with $a=0.2$ and $b=7$ whereas the dotted line is the power law of Eq. (15). Inset: enlargement of the $Q\ll Q_0$ zone where the values of $\bar{H_s}/D$ have been added in open symbols.

$$\frac{H_s}{\lambda_0}\simeq 0.25\left(\frac{Q}{Q_0}\right)^{1.5}. \tag{15}$$

Note that Eq. (15) can also be expressed as

$$\frac{H_s}{D}\simeq 0.25\left(\frac{U}{U_0}\right)^{1.5}, \tag{16}$$

where $U=Q/D^2$ is proportional to the injection velocity and where $U_0=(\nu g^*)^{1/3}$ appears as a characteristic velocity although we do not have any simple physical interpretation for it. Just note that when looking for a relation between H_s and U by dimensional analysis, the physical parameters are D, g^*, and ν. Then, if we assume that H_s is simply proportional to D, as suggested by the experiments, U_0 is the only relevant choice to construct a characteristic velocity with ν and g^*.

VII. DISCUSSION AND CONCLUSION

A. Dimensionless numbers

Up to now, we have drawn our interpretation on a theoretical model which can very satisfactorily predict most of the experimental observations and measurements. But these results can also be interpreted in terms of dimensionless numbers. Two of them seem particulary relevant in this problem: the Reynolds number Re and the Froude number Fr. Re characterizes the competition between convective and viscous effects in the flow at the injection. It is built with $U=Q/D^2$ and D as velocity and length scales at the nozzle end:

$$\mathrm{Re}=\frac{UD}{\nu}=\frac{Q}{\nu D}.$$

Fr compares kinetic energy to gravitational energy. Taking into account the resultant density, i.e., gravity and negative buoyancy, and the depth of penetration H_s, we obtain

$$\mathrm{Fr}=\frac{\rho U^2}{\Delta\rho g H_s}=\frac{Q^2}{g^* H_s D^4}.$$

Some authors use D instead of H_s in the definition of Fr or of the Richardson number Ri. This number, already mentioned in the Introduction, is frequently used in the context of turbulent jets or plumes and reads

$$\mathrm{Ri}=\frac{g^* D}{U^2}=\frac{g^* D^5}{Q^2}.$$

Here we preferred to choose H_s as gravitational length scale because, contrary to D, it corresponds to the real displacement performed by the lighter liquid from the nozzle of injection down to the head of the jet.

In addition to these three dimensionless groups, another number comes very naturally from the model and was already defined in Eq. (13):

$$S=\frac{\nu U}{g^* D^2}=\frac{\nu Q}{g^* D^4}.$$

This number compares the viscous friction to the resultant gravity force and is a combination of the Reynolds and Richardson numbers: $S=(\mathrm{Re\,Ri})^{-1}$. It should be noticed that, contrary to the other numbers which compare opposite effects, the viscous and buoyancy terms used in S act together in the same direction. So S predicts whether the slowing-down of the flow from the nozzle down to the jet's cap is mainly due to the viscous friction ($S\gg1$), to the negative buoyancy ($S\ll1$) or to both of them ($S\sim1$). It can be seen as the inverse of the Poiseuille number or also as the Reynolds number divided by the Galileo number. Anyway, this number has already been used by different authors in the context of a liquid moving in an outer miscible liquid[17] and it appears to be a very relevant parameter in this particular situation.

Now, it is possible to check any dependency between these dimensionless numbers. Then, as shown in Fig. 9, a strong correlation is obtained between the Froude number Fr and the parameter S. Using Eq. (12) in the expression of Fr, one simply obtains from the model

$$\mathrm{Fr}=\frac{S}{a\ln(1+bS)}. \tag{17}$$

This equation is presented in solid line in Fig. 9 with the typical values of the parameters $a=0.2$ and $b=7$; it is in very good agreement with the experimental data. Note that the constant value of Fr in the inviscid limit ($S\ll1$) corresponds simply to the Bernoulli relation, $\Delta\rho g H_s=\frac{1}{2}\rho\alpha V(0)^2$, where the kinetic energy is fully converted in potential energy.

Here again, the data can be satisfactory described in nearly the whole experimental range by a power law in S. Equations (15) and (16) suggest an exponent close to $1/2$. In fact, the best agreement is obtained with an exponent 0.6 and gives the following empirical law:

$$\mathrm{Fr}\approx 3.5\,S^{0.6}. \tag{18}$$

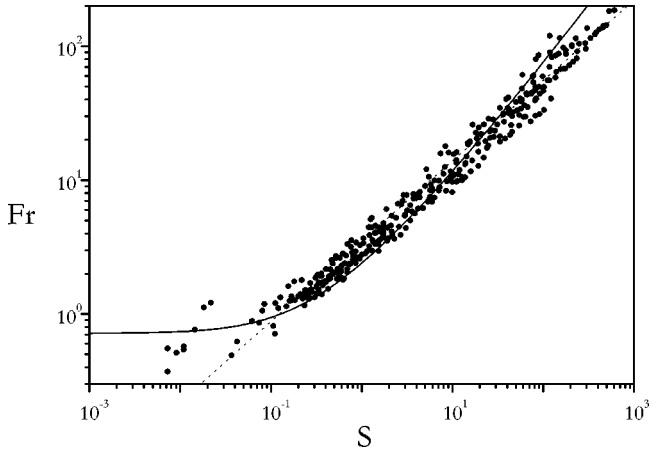

FIG. 9. Same points as in Fig. 8 (with $\overline{H_s}$ instead of H_s for $S<2\times10^{-2}$) but plotted in terms of dimensionless numbers: Fr as a function of S. The solid line corresponds to the model prediction with parameters $a=0.2$ and $b=7$ whereas the dotted line is a power law with an exponent 0.6 slightly larger than $1/2$.

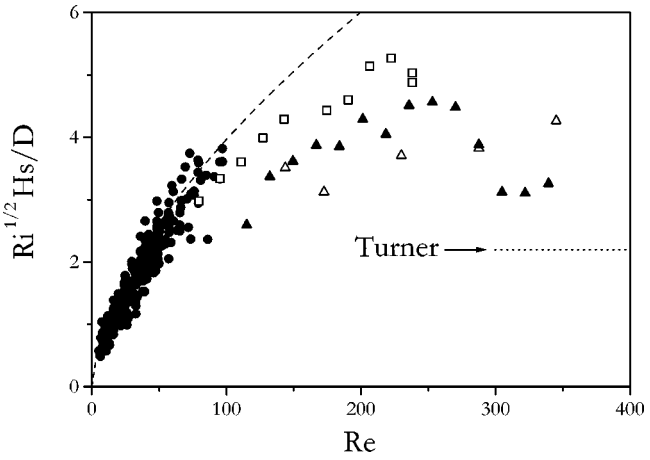

FIG. 10. Plot of $\mathrm{Ri}^{1/2}\ H_s/D$ vs the Reynolds number Re for all the experimental data previously collected (●) and for three experiments with higher values of Re: $D=0.175$ cm, $\Delta\rho/\rho=2.59\times10^{-2}$, and $\nu=\nu_0$ (□); $D=0.483$ cm, $\Delta\rho/\rho=6.98\times10^{-3}$, and $\nu=\nu_0$ (▲); and $D=0.483$ cm, $\Delta\rho/\rho=2.59\times10^{-2}$, and $\nu=\nu_0$ (△). The turbulent limit deduced from Turner's law is shown in dotted line and is approximately equal to 2.21. The previously collected data (●) are well fitted by a power law with an exponent $\phi=0.6$ and shown here in dashed line.

B. From laminar to turbulent jets

The comparison between our results and previous works is difficult since only very few studies have been carried out in the laminar situation, in miscible or immiscible conditions.[2,3,9,10] Furthermore they were all restricted to the case of very small penetration ratio ($H/D<2$). Then, the horizontal length scale is comparable to the vertical length scale and the situation is totally different in terms of physical mechanisms involved. Contrary to the laminar situation, the case of turbulent jets or plumes has been extensively studied and quite a general consensus seems to be reached: indeed, it appears that the penetration ration H/D is strongly correlated to the Richardson number Ri. For small values of Ri, i.e., $\mathrm{Ri}<1$, an empirical power law with an exponent $-1/2$ was first proposed by Turner[4,5] and can be written as follows:

$$\frac{H}{D}\approx 2.21\ \mathrm{Ri}^{-1/2}. \tag{19}$$

This expression is also consistent with a dimensional analysis.[4,5]

We have seen in the previous sections that our experimental results as well as our model do not predict such a relation. Nevertheless, from the empirical laws of both Eqs. (15) and (18), we can obtain approximately the same dependence on Ri but with an extra dependence on Re with an exponent $\phi\sim0.5-0.6$:

$$\frac{H_s}{D}\approx 0.25\ \mathrm{Re}^{\phi}\mathrm{Ri}^{-1/2}. \tag{20}$$

As we have also worked with Richardson numbers smaller than 1, we can compare these results in terms of Reynolds number, from the small values used in our laminar experiments ($\mathrm{Re}<100$) to the fully established turbulent flow with Reynolds numbers larger than 1000. So, we can infer that between these two limit behaviors a progressive transition from laminar to turbulent takes place. Then the jet gradually loses its dependence in Reynolds number while viscous friction becomes totally insignificant in comparison to inertial effects.

To analyze this transition more precisely, we have performed few additional experiments where the Reynolds number was increased up to about 350, the maximal value that can be reached in our setup. The influence of the Reynolds number on the penetration ratio can be clearly underlined by plotting $\mathrm{Ri}^{1/2}\ H_s/D$ as a function of Re. The results are presented in Fig. 10 where we have also added the previous experimental data (Figs. 8 and 9) as well as the turbulent limit obtained by Turner and which corresponds to an approximate value of 2.21.[4,5] When the flow becomes turbulent, H_s corresponds no more to the stationary depth but to the mean penetration depth because the jet fluctuates more or less intensively.

As expected from Eq. (20), in the small Re zone, the data are satisfactory fitted by a power law with an optimal exponent $\phi=0.6$. For larger values of Re, the experimental points progressively deviate from this power law and do not collapse anymore when $\Delta\rho/\rho$ or D is changed. All these points as well as part of the previously collected data correspond to values of $\mathrm{Ri}^{1/2}\ H_s/D$ larger than the turbulent limit of 2.21. During the transition from laminar to turbulent flow, this quantity first increases until it progressively stabilizes before starting to decrease. Finally, for high values of Re, it should reach Turner's limit. So, from the relative positions of the three experimental curves observed in Fig. 10 at $\mathrm{Re}>100$, we can infer that the transition to turbulence is produced more easily for a larger diameter of injection D and for a higher difference of density $\Delta\rho/\rho$. This can be rather well understood since the physical mechanism of this transition might be due to Kelvin–Helmholtz instabilities which are more likely to appear in a jet with a big diameter or with a large contrast of density. Finally, one curve ($D=0.483$ cm and $\Delta\rho/\rho=6.98\times10^{-3}$) reveals that the transition is at first

progressive and then becomes very sharp: indeed, at Re ~ 280, the quantity $\mathrm{Ri}^{1/2}\, H_s/D$ falls abruptly down to a value rather close to the turbulent limit. For the two other curves, we believe that a similar sharp transition might take place for values of Re larger than those accessible here. With a suitable setup, this procedure could be used to study more in-depth the transition from laminar to turbulent flow in a vertical liquid jet.

C. Conclusion

We have presented an extensive study of negatively buoyant jets injected in a miscible liquid. Almost all experiments were performed in laminar conditions. They revealed a transient penetration followed by a subsequent steady state with a constant penetration depth. Based on two practical assumptions, a theoretical model is proposed which accounts for the transient phase and for the final penetration depth as well as the stationary profile of the jet. The agreement between the measurements and the model was very satisfactory and seems to confirm the assumptions made. In particular, a general relation between the densimetric Froude number and the number S comparing viscous to buoyant effects is obtained both theoretically and experimentally. Finally, these results have been profitably compared to previous studies of turbulent plumes: our analysis suggests that the transition from laminar to turbulent flow is characterized by the penetration ratio H_s/D which progressively evolves from a double dependence on $\mathrm{Re}^{1/2}$ and $\mathrm{Ri}^{-1/2}$ to a single dependence on $\mathrm{Ri}^{-1/2}$.

ACKNOWLEDGMENTS

The authors are grateful to J. Snoeijer and J. Bico for a careful reading of the manuscript. The authors would like to acknowledge the financial support of the CNES (Centre National d'Etudes Spatiales), especially one of them, P.Ph., who benefits from a postdoctoral fellowship.

[1] L. Pantzlaff and R. M. Lueptow, "Transient positively and negatively buoyant turbulent rounds jets," Exp. Fluids **27**, 117 (1999).
[2] P. D. Friedman and J. Katz, "The flow and mixing mechanisms caused by the impingement of an immiscible interface with a vertical jet," Phys. Fluids **11**, 2598 (1999).
[3] P. D. Friedman and J. Katz, "Rise height for negatively buoyant fountains and depth of penetration for negatively buoyant jets impining an interface," J. Fluids Eng. **122**, 779 (2000).
[4] W. D. Baines, J. S. Turner, and I. H. Campbell, "Turbulent fountains in an open chamber," J. Fluid Mech. **212**, 557 (1990).
[5] J. S. Turner, "Jets and plumes with negative or reversing buoyancy," J. Fluid Mech. **26**, 779 (1966).
[6] B. R. Morton, "Forced plumes," J. Fluid Mech. **5**, 151 (1959).
[7] L. J. Bloomfield and R. C. Kerr, "A theoretical model of a turbulent fountain," J. Fluid Mech. **424**, 197 (2000).
[8] R. W. Cresswell and R. T. Szczepura, "Experimental investigation into a turbulent jet with negative buoyancy," Phys. Fluids A **5**, 2865 (1993).
[9] W. Lin and S. W. Armfield, "Direct simulation of weak axisymmetric fountains in a homogeneous fluid," J. Fluid Mech. **403**, 67 (2000).
[10] W. Lin and S. W. Armfield, "The Reynolds and Prandtl number dependence of weak fountains," Comput. Mech. **31**, 379 (2003).
[11] R. A. Seban, M. M. Behnia, and K. E. Abreau, "Temperatures in a heated air jet discharged downward," Int. J. Heat Mass Transfer **21**, 1453 (1978).
[12] C. Clanet, "On large amplitude pulsating fountain," J. Fluid Mech. **366**, 333 (1998).
[13] D. J. Tritton, *Physical Fluid Dynamics*, 2nd ed. (Clarendon, Oxford, 1988).
[14] E. Moses, G. Zocchi, and A. Libchaber, "An experimental study of laminar plumes," J. Fluid Mech. **251**, 581 (1993).
[15] G. Schubert, D. L. Turcotte, and P. Olson, *Mantel Convection in the Earth and Planets* (Cambridge University Press, Cambrige, 2001).
[16] R. Comolet, *Mécanique Expérimentale des Fluides, Tome I* (Dunod, Paris, 1990).
[17] P. Petitjeans and T. Maxworthy, "Miscible displacement in capillary tubes," J. Fluid Mech. **326**, 37 (1996).